Engineering and Applied Science Letters

PSR Press

Article

Optimization and mechanistic assessment of chromium ion removal from brewery effluent using African pear (*Dacryodes edulis*) seed activated carbon

Ukpong Anwana Abel[1,*], Uzono Romokere Isotuk[1], Okon Godwin Okon[2], Antia Ukponobong[3], Okon Joseph Etim[2], Akwayo Iniobong Job[1], Umoren Godwin Ani[1] and Ebong Ekemini Paul[1]

[1] Department of Chemical and Petrochemical Engineering, Akwa Ibom State University, Ikot Akpaden, Mkpat Enin L.G.A, Nigeria
[2] Department of Botany, Akwa Ibom State University, Ikot Akpaden, Mkpat Enin L.G.A, Nigeria
[3] Department of Microbiology, Akwa Ibom State University, Ikot Akpaden, Mkpat Enin L.G.A, Nigeria
* Correspondence: anwanaukpong@aksu.edu.ng

Received: 16 April 2026; Accepted: 05 June 2026; Published: 22 June 2026.

Abstract: Brewery effluent may have dissolved heavy metals that remain in the receiving waters and affect both aquatic life and human health. This study explored the efficiency of the African pear seed activated carbon (APSAC) derived from *Dacryodes edulis* seed waste as a low-cost adsorbent for removing chromium ion (Cr^{2+}) from brewery wastewater. APSAC was synthesized by the procedure involving drying and pulverization of the seed waste, carbonization at 600 °C for 2 h, 40% H_2SO_4 impregnation for 24 h, activation at 500 °C for 4 h, neutral washing, drying, and sieving into 250 μm fraction. Proximate analysis, Fourier-transform infrared spectroscopy, and scanning electron microscopy were employed for characterizing bulk properties, surface functional groups, and surface morphology. Batch experiments of the adsorption process were planned on the basis of central composite design to investigate the influence of contact time (15–75 min), initial Cr^{2+} concentration (0.005–0.025 mg L^{-1}), and adsorbent dosage (0.5–2.5 g). The maximum Cr^{2+} removal observed was 96% at 0.025 mg L^{-1}, 1.5 g APSAC, and 45 min, while the maximum adsorption capacity of APSAC was 0.0048 mg g^{-1} at 0.015 mg L^{-1}, 0.5 g APSAC, and 45 min. The developed model for the adsorption capacity response was statistically significant ($F = 13.94$, $p = 0.0049$) and had high explanatory power ($R^2 = 0.9617$). The equilibrium data were better described by the Sips isotherm model ($R^2 = 0.9849$) indicating the heterogeneity of surface adsorption process. The kinetic and Boyd studies suggested that surface absorption and film diffusion controlled the process of chromium removal rate. The results confirm the effectiveness of APSAC as biomass-derived adsorbent for chromium removal from brewery effluent and the potential of valorization of the African pear seed waste in wastewater treatment.

Keywords: African pear seed activated carbon, adsorption, brewery effluent, chromium ion, response surface methodology, sips isotherm, Boyd model, biomass valorization

1. Introduction

Industrial effluent is wastewater generated during processing in industries such as mining, electroplating, leather tanning, pigments and dyes, ceramics, breweries, food processing, oil exploration and pharmaceuticals [1–7]. Large amount of water is required by breweries in the processes of brewing, washing, cooling, bottling and cleaning purposes and the wastewater contains suspended solids, organic load, dissolved salts and metal elements such as chromium, cadmium, copper, lead, nickel and iron [8,9]. The release of such effluents into water bodies may affect water quality through changing the pH level, reducing light penetration, disrupting dissolved oxygen balance and creating hazards because heavy metals are not biodegradable and tend to bioaccumulate in both organisms and soils [10].

Metal pollution in the environment has drawn much concern because metal-bearing effluents could pose danger to the ecosystem and human health even at low concentrations. The conventional technologies in the treatment of wastewater containing toxic metal ions are chemical precipitation, flotation, ion exchange and membrane filtration [11–14]. Despite their efficiencies, high operating costs, production of secondary sludge,

regeneration difficulties and membrane fouling are some of the constraints associated with these technologies. Adsorption has continued to attract much interest because of its simplicity of operation, suitability to batch and continuous process as well as compatibility with inexpensive sorbents derived from biomass [15,16].

Activated carbon has remained among the most popular adsorbent for the removal of metal ions and organic compounds due to its porous structure, surface functional groups and relatively high affinity to dissolved contaminants. Biomass materials including coconut shells, coconut coir, rice husks, orange peels, peanut husks, sawdust, prickly pear seed cake and many others have been transformed into activated carbon for wastewater treatment [1,2,15–19]. The process not only removes the pollutants but also finds value for the use of the agro-residues. Agro-wastes of African pear (*Dacryodes edulis*) seeds have been reported in parts of Nigeria, although its transformation into activated carbon for chromium removal from brewery effluent has not been extensively studied.

In the present study, the use of activated carbon obtained from the local agro-waste of African pear seeds is proposed for the removal of Cr^{2+} from brewery effluent. The novelty of this research involves the combination of the preparation of African pear seed activated carbon (APSAC), physicochemical characterization and the determination of optimum condition, equilibrium isotherm and kinetics under the same experimental conditions. The aims of the research were the preparation and characterization of APSAC, the assessment of the effect of contact time, initial Cr^{2+} concentration and adsorbent dosage on chromium removal and adsorption capacity, the identification of the most suitable isotherm for the equilibrium data and the elucidation of the rate controlling mechanism.

2. Experimental methods

2.1. Materials

Seeds of the African pear tree that served as the activated-carbon precursor were sourced from Ikot Akpaden, Mkpat Enin Local Government Area, Akwa Ibom State, Nigeria. Sulphuric acid (H_2SO_4) was purchased from a chemical vendor in Uyo, Akwa Ibom State, Nigeria. Brewery effluent was acquired from Champions Breweries PLC, Uyo, Akwa Ibom State, Nigeria. Distilled water was used in cleaning, preparation and neutralization processes.

2.2. Preparation of APSAC

The African pear seeds were cleaned several times with distilled water to eliminate any adhering impurities and allowed to dry under the sun for 3 days. The dried seeds were pulverized to decrease particle size and oven-dried at 100 °C for 4 h. The precursor was carbonized in the muffle furnace (GALLENKAMP 220/240) at 600 °C for 2 h. The carbonized material was soaked in 40% concentrated H_2SO_4 for 24 h and activated in the muffle furnace at 500 °C for 4 h. The activated product was washed with distilled water till a neutral pH of 7.0 was attained and was dried at 100 °C for 4 h. It was then sieved to obtain particle size of 250 μm. The sieved product was kept in an airtight container before use.

2.3. Proximate analysis of the adsorbent

The physicochemical characteristics of APSAC were determined by standard ASTM procedure [20]. The determination of moisture content, volatile matter, ash content, bulk density and pH were done based on ASTM D2867, ASTM D2865, ASTM D2866, ASTM D2854-96 and ASTM D3838-80 standards respectively. Fixed carbon was evaluated from mass balance after determination of moisture, volatile matter and ash contents.

2.4. Characterization of the adsorbent

Surface morphology of the adsorbent before and after adsorption were analyzed by means of scanning electron microscopy (SEM; JEOL JSM-6300F). Identification of surface functional groups were done using FTIR (Perkin-Elmer Spectrum 2000) in the mid-infrared region. The procedures for characterizing the adsorbent followed those described in literature [20,21].

2.5. Batch adsorption experiments

Batch studies were conducted to study the effect of contact time, initial chromium concentration and adsorbent dose on chromium adsorption on APSAC. In each experiment, 200 mL of chromium containing brewery effluent or prepared metal ion solution was taken in a 250 mL beaker and a certain quantity of APSAC was introduced. The beaker was agitated on an orbital shaker (Rotamax 120, Heidolph) at 150 rpm and 25 °C for a specific contact time. The suspension was filtered with Whatman No. 14 filter paper and the chromium residual concentrations were measured using atomic absorption spectroscopy (Unicam Thermo/Solar System 2009 model). The chromium equilibrium uptake capacity, uptake rate at any time t and percentage removal of chromium were calculated according to Equations (1)–(3).

$$q_e = \frac{(C_o - C_e)V}{M}, \tag{1}$$

$$q_t = \frac{(C_o - C_t)V}{M}, \tag{2}$$

$$\%\,\text{removal} = \frac{(C_o - C_e)}{C_o} \times 100. \tag{3}$$

In the above equations, C_o represents the initial chromium concentration (mg L^{-1}), C_e represents the equilibrium concentration (mg L^{-1}), C_t is the concentration at time t (mg L^{-1}), V is the volume of the solution (L), and M is the mass of the adsorbent (g). The procedure followed in the preparation of adsorbents, adsorption process, filtration, and analytical measurement is illustrated in Fig. 1.

Figure 1. Experimental procedure of APSAC preparation, batch adsorption, filtration, and instrumental analysis

2.6. Design of experiment

The adsorption tests have been designed using central composite design in Design-Expert software version 10 to study the effect of three factors on adsorption capacity and the removal of chromium. Factors such as contact time (A), initial chromium concentration (B), and adsorbent dosage (C) have been varied within the ranges specified in Table 1. Table 2 shows the designed experimental matrix and corresponding responses. Response surface method has been employed to explain the effect of factors on the adsorption response and the quadratic model was analyzed through ANOVA.

Table 1. Independent variables and experimental ranges used in the central composite design

Factor	Variable	Type	Minimum	Maximum
A	Contact time (min)	Numeric	15	75
B	Initial concentration (mg L^{-1})	Numeric	0.005	0.025
C	Adsorbent dosage (g)	Numeric	0.5	2.5

Table 2. Central composite design matrix and observed adsorption responses for Cr^{2+} removal

Run	Factor *A* Contact time (min)	Factor *B* Initial concentration ($mg\,L^{-1}$)	Factor *C* Adsorbent dosage (g)	Adsorption capacity ($mg\,g^{-1}$)	Cr^{2+} removal (%)
1	30	0.020	2.0	0.001700	85.0000
2	60	0.010	2.0	0.000200	20.0000
3	30	0.020	1.0	0.003800	95.0000
4	45	0.015	0.5	0.004800	80.0000
5	30	0.010	1.0	0.001000	50.0000
6	15	0.015	1.5	0.001467	73.3333
7	75	0.015	1.5	0.001867	93.3333
8	45	0.005	1.5	0.000533	80.0000
9	45	0.015	2.5	0.001120	93.3333
10	60	0.020	2.0	0.001700	85.0000
11	30	0.010	2.0	0.000500	50.0000
12	45	0.025	1.5	0.003200	96.0000
13	45	0.015	1.5	0.000533	26.6667
14	60	0.010	1.0	0.001400	70.0000
15	60	0.020	1.0	0.003000	75.0000

3. Results and Discussion

3.1. Physico-chemical properties of APSAC

Proximate properties of APSAC are shown in Table 3. The sample had a low percentage of moisture (3.28%) and a low ash percentage (1.28%), suggesting that drying, carbonization and activation processes produced a carbon-enriched adsorbent having little inorganic ash. Low moisture content is preferred since the water filling pores would reduce the adsorption capacity. Ash can be detrimental due to pore blockage, reduction in concentration of active carbon and decrease in strength and activity of activated carbons [20,21]. Volatile matter of 1.04% is an indication of elimination of most of the thermally unstable compounds, resulting in the production of relatively stable carbon matrix. Density of $0.332\,g\,cm^{-3}$ indicates that the sample could settle well and contact the water system. The close to neutral pH (7.02) is an indicator of minimal disturbance in pH of the system during treatment process. The fixed carbon content of 86.0% confirms that APSAC possesses a carbon-rich structure suitable for contaminant uptake.

Table 3. Physicochemical properties of APSAC

Property	APSAC
Moisture content (%)	3.28
Volatile matter (%)	1.04
Ash content (%)	1.28
pH	7.02
Bulk density ($g\,cm^{-3}$)	0.332
Fixed carbon (%)	86.0

3.2. Surface morphology of APSAC

The SEM images prior to and post-adsorption are presented in Figure 2. It can be observed that the surface of raw APSAC in Figure 2(a) has an uneven surface topography with irregular particles, rough surfaces, and cavities as a result of the acid activation process. These characteristics of the surface are favorable since they provide more surface areas for the chromium adsorption. In Figure 2(b), it can be seen that the surface after adsorption has relatively more coverage, and there are cavities which are partially occupied. This is a morphological modification that confirms the uptake of chromium on APSAC and is in agreement with the pore filling, surface complexing, and deposition of adsorbed species observed in biomass-based activated carbons [17–19,22].

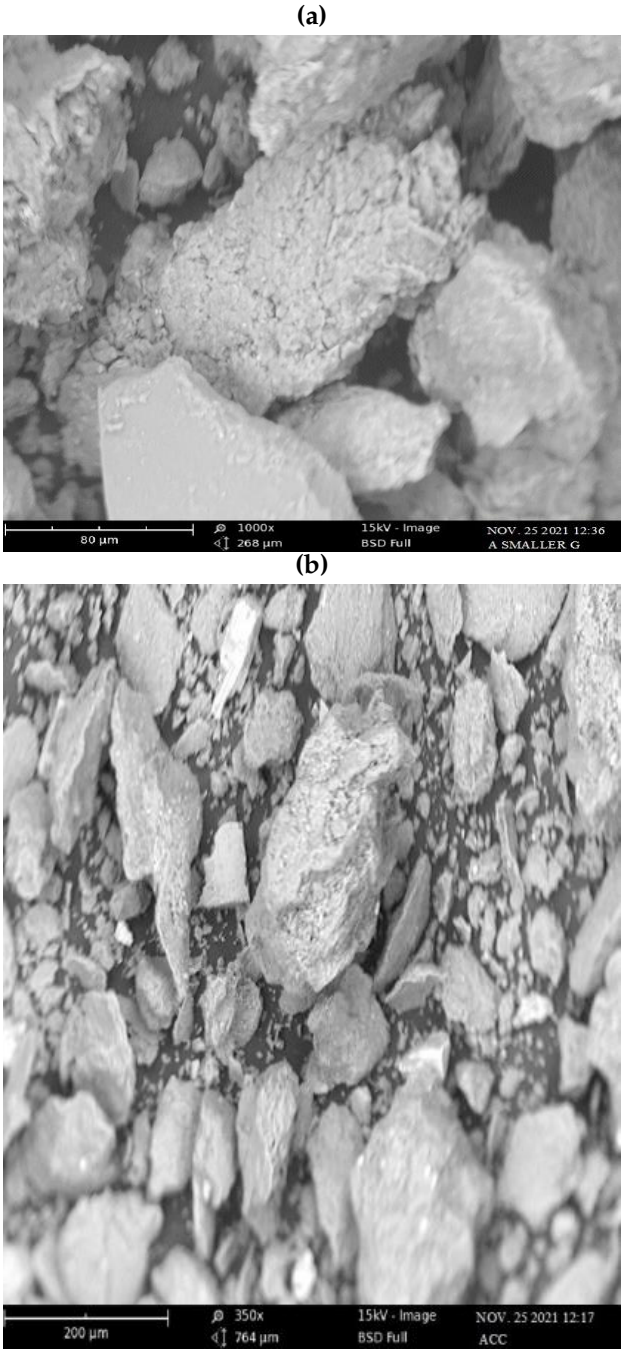

Figure 2. SEM micrographs of APSAC: (a) before adsorption and (b) after Cr^{2+} adsorption

3.3. FTIR Studies on APSAC

The FTIR spectra given in Figure 3 along with the assignment data given in Table 4 reveal that APSAC has oxygen-containing and carbon-containing functional groups that can react with chromium species. Prior to adsorption, the broad band ranging from 3564.57 to 3248.23 cm^{-1} suggests the presence of hydrogen-bonded hydroxyl groups, and the peak at 1712.85 cm^{-1} is due to stretching vibration of carbonyl groups of carboxylic acid group. The peaks at 1211.34 and 918.15 cm^{-1} are suggestive of C-O/C-O-C and O-H out-of-plane vibrations respectively, indicating the presence of oxygen-containing surface sites.

Upon adsorption, the spectrum shows a prominent OH group at 3419.90 cm^{-1}, a peak at 1641.48 cm^{-1} that can be either due to C=C stretching or N-H bending vibration and peaks at 675.11-611.45 cm^{-1} corresponding to inorganic or metal-oxygen vibrations. The reduction or absence of some peaks before and after adsorption, specifically carboxyl or carbonyl groups, is an indication that oxygenated sites have taken part in the binding

of chromium. These spectral changes support a multi-site adsorption process involving surface functional groups rather than simple physical retention alone [23,24].

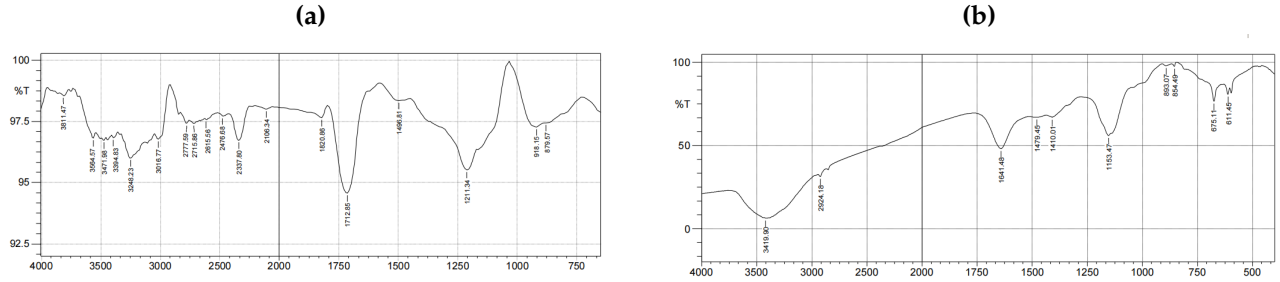

Figure 3. FTIR spectra of APSAC: (a) before adsorption and (b) after Cr^{2+} adsorption

Table 4. FTIR peak assignments for APSAC before and after adsorption

Functional group assignment	Before adsorption (cm^{-1})	After adsorption (cm^{-1})
O–H stretching of alcohol groups	3811.47	–
Hydrogen-bonded O–H stretching of alcohol, carboxylic acid, or phenol groups	3564.57–3248.23	3419.90
=C–H stretching of aromatic groups	3016.77	–
Asymmetric C–H stretching of aliphatic CH\textsubscript{2}/CH\textsubscript{3} groups	–	2924.18
Asymmetric C–H stretching of aldehyde groups	2777.59–2715.86	–
O–H stretching of carboxylic acid groups	2615.56	–
S–H stretching, P–H stretching, or carboxylic-acid O–H vibration	2476.68	–
C≡C stretching of alkyne groups	2106.34	–
C=O stretching of aryl carbonate groups	1820.86	–
C=O stretching of carboxylic acid groups	1712.85	–
C=C stretching of alkene groups or N–H bending of primary amine/amide groups	–	1641.48
C=C stretching of aromatic rings or N–H bending	1498.81	–
C–H bending of aliphatic methylene groups	–	1479.45
C–H bending or O–H in-plane bending of alcohol/carboxylate groups	–	1410.01
C–O–C stretching of ethers/esters or C–O stretching of carboxylic acid groups	1211.34	1153.47
O–H out-of-plane bending of carboxylic acid dimers	918.15	–
C–H out-of-plane bending of substituted aromatic rings	879.57	893.07–854.49
C–X or metal–oxide stretching of inorganic components	–	675.11–611.45

3.4. Modelling the effect of the factors on chromium removal and adsorption capacity

It can be noted from the experimental results shown in Table 2 that APSAC efficiency depended greatly on the interaction between the contact time, the concentration of the ions, and the adsorbent dosage. The highest chromium removal percentage was 96% at 45 min, 0.025 mg L^{-1}, and 1.5 g APSAC, while the highest adsorption capacity was 0.0048 mg g^{-1} at 45 min, 0.015 mg L^{-1}, and 0.5 g APSAC. It is necessary to mention the difference between the two parameters as the increase in percentage of chromium removed means more adsorption sites available. The adsorption capacity, however, is dependent on the dosage, as the sites not being used reduce the amount of chromium adsorbed per unit mass of the sorbent. Therefore, in the optimal case one should choose the design depending on the goal of the experiment: polishing of the water or utilization of the sorbent.

3.5. ANOVA and regression model of adsorption capacity

ANOVA table of the adsorption capacity response is shown in Table 5. It can be seen that the quadratic model of the response is significant ($F = 13.94$, $p = 0.0049$). This implies that the chosen factors accounted for the variation observed in the experiment. The high value of the coefficient of determination ($R^2 = 0.9617$) was supported by the adjusted R^2 value of 0.8927, thus demonstrating that the selected model still retains its explanatory power with respect to the number of terms included in the model. The smaller predicted R^2 of 0.6690 is expected in the case of small design experiments within limited concentration range. The adequate precision of 11.8203 was higher than 4 (Table 6).

Table 5. ANOVA for the adsorption-capacity response

Source	Sum of squares	df	Mean square	*F*-value	*p*-value	Significance
Model	2.43E-05	9	2.70E-06	13.94	0.0049	Significant
A – Contact time	3.81E-07	1	3.81E-07	1.97	0.2193	–
B – Initial concentration	1.74E-08	1	1.74E-08	0.0897	0.7767	–
C – Adsorbent dosage	2.71E-06	1	2.71E-06	13.99	0.0134	Significant
AB	1.01E-07	1	1.01E-07	0.5231	0.5019	–
AC	1.25E-09	1	1.25E-09	0.0065	0.9391	–
BC	3.61E-07	1	3.61E-07	1.87	0.2301	–
A^2	9.56E-07	1	9.56E-07	4.94	0.0769	–
B^2	1.31E-06	1	1.31E-06	6.76	0.0482	Significant
C^2	4.22E-06	1	4.22E-06	21.80	0.0055	Significant
Residual	9.68E-07	5	1.94E-07	–	–	–
Corrected total	2.53E-05	14	–	–	–	–

Table 6. Fit statistics for the adsorption-capacity model

Metric	Value
Standard deviation	0.0004
Mean	0.0018
Coefficient of variation (%)	24.6
R^2	0.9617
Adjusted R^2	0.8927
Predicted R^2	0.6690
Adequate precision	11.8203

The significant factors in Table 5 were the adsorbent dosage (C), the quadratic concentration factor (B^2), and the quadratic dosage factor (C^2). Such result reveals that the adsorption capacity was not dependent on a simple linear increase in sorbent weight. Rather, the curvature factors reveal a non-linear relationship between available binding sites, driving force of the solute, and adsorbent usage. The quadratic model for adsorption capacity using coded factors is given in Eq. (4). The factors A, B, and C in the equation refer to the coded contact time, initial chromium concentration, and adsorbent dosage, respectively.

$$\begin{aligned} q_e = {} & 4.496 \times 10^{-4} + 6.250 \times 10^{-6} A + 7.771 \times 10^{-4} B - 7.788 \times 10^{-4} C \\ & - 1.125 \times 10^{-4} AB + 1.250 \times 10^{-5} AC - 2.125 \times 10^{-4} BC \\ & + 2.938 \times 10^{-4} A^2 + 3.438 \times 10^{-4} B^2 + 6.171 \times 10^{-4} C^2. \end{aligned} \tag{4}$$

3.6. Interactions and impacts on chromium removal

The response surfaces presented in Figure 4 give information on the joint effect of operating parameters on chromium removal. It was noted that an increase in the amount of adsorbent generally increased the removal rate since the use of more APSAC meant having more adsorption sites. However, from the response surfaces, it is clear that the effect of increasing dosage was not consistent, especially with different initial concentrations of chromium ions. In the case of high initial concentration, the presence of strong driving force meant better contact and, hence, adsorption; however, there was increased competition among adsorbing species. Thus, the optimum range was in the intermediate-to-high dosage level coupled with enough contact time.

Contact time changed the above behavior by increasing the surface coverage. Removal increased with contact time approaching the middle-to-high range, beyond which the response surface started flattening due to the process approaching equilibrium. The interactions between contact time and initial concentration demonstrate that rapid removal could be obtained when the initial concentration was low; otherwise, adequate time was required for diffusion through the boundary layer and adsorption onto the active sites. The findings are consistent with the statistical response and kinetics results in which the influence of external mass transfer is observed [25,26].

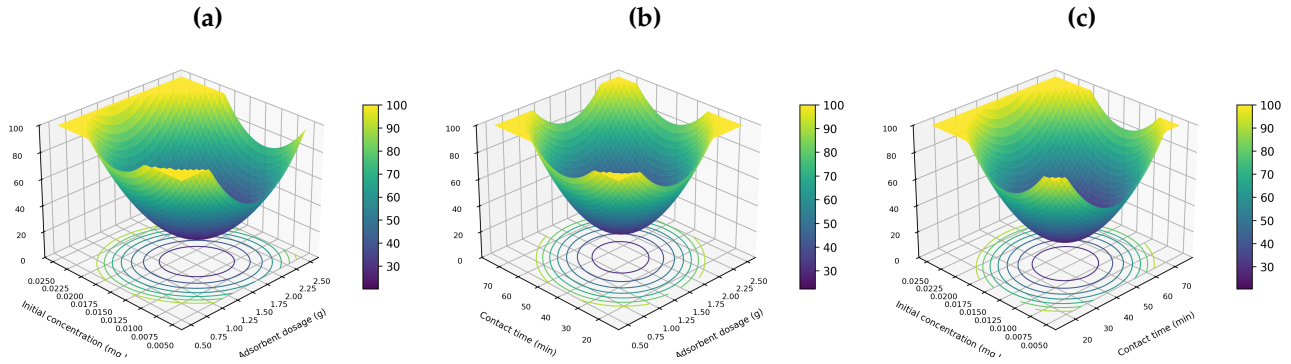

Figure 4. Response surfaces for Cr^{2+} removal: (a) adsorbent dosage and initial concentration at 45 min; (b) adsorbent dosage and contact time at 0.015 mg L^{-1}; and (c) contact time and initial concentration at 1.5 g APSAC

3.7. Interactions influencing the adsorption capacity

From the adsorption capacity surfaces presented in Figure 5, a reaction trend is observed to be different from percentage removal due to capacity being defined per mass of adsorbent. When contact time is constant, increase in the initial concentration promoted the adsorption capacity through the increased concentration gradient between the solution and the APSAC surface. However, increased adsorbent dosage caused reduction in mass-based adsorption capacity in some regions since the same amount of chromium was spread on a higher mass of adsorbent. This explains why the highest percentage removal and highest adsorption capacity occurred at different experimental conditions.

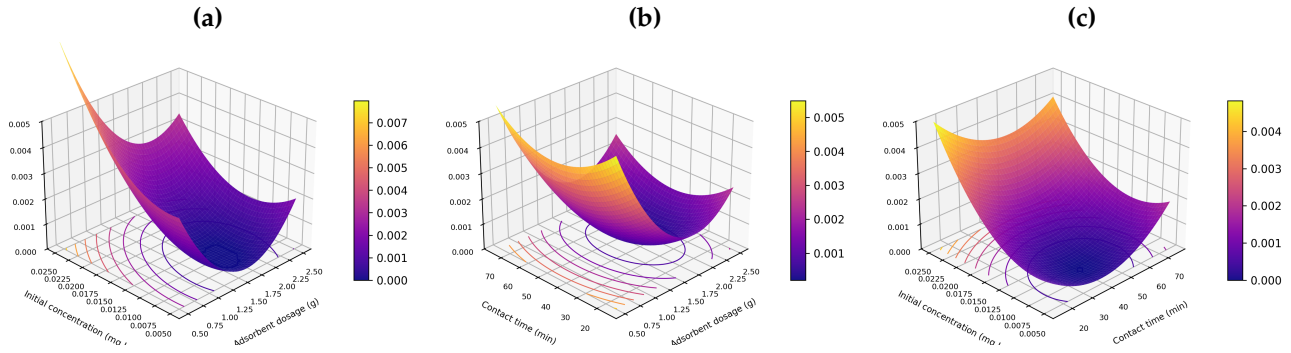

Figure 5. Response surfaces for adsorption capacity: (a) adsorbent dosage and initial concentration at 45 min; (b) adsorbent dosage and contact time at 0.015 mg L^{-1}; and (c) contact time and initial concentration at 1.5 g APSAC

As seen from the capacity vs. dosage/concentration and capacity vs. contact-time plots, the effect of dose/concentration was significantly stronger than that of time in the analyzed region. This result implies that quite a significant amount of chromium had been accumulated by the material before the maximum time of contact had elapsed, whereas further shaking would lead to an improvement in the completeness of coverage of the surface rather than a linear growth in mass-normalized capacity. This information is important when choosing the optimal conditions for application of the sorbent.

3.8. Adsorption isotherm

Adsorption isotherms obtained from the equilibrium state were fitted using Langmuir, Freundlich, Sips and Redlich-Peterson isotherm models (Table 7). According to the Langmuir model, $q_m = 0.2623$ mg g^{-1}, $b = 2.4367$ L mg^{-1} and $R^2 = 0.9106$. Thus, there was a moderately good agreement between the experimental data and the assumption of monolayer adsorption on the homogeneous surface. As per the Freundlich model, $R^2 = 0.9165$ and the intensity parameter was equal to $n = 0.9035$. It can be concluded that the adsorption surface was not a uniform heterogeneous surface as it could be expected for this adsorption mechanism [27,28].

Sips model was found to give the best fits with the parameters $R^2 = 0.9849$, $q_{ms} = 0.00697$ mg g^{-1}, $K_s = 1.124 \times 10^7$, and $\beta = 3.0859$. Since Sips model is characterized by the combination of Langmuir-like

saturation with Freundlich-like heterogeneity, the good fit obtained can be interpreted to mean that there are binding sites on APSAC that differ in their affinity for Cr(VI). This result supports the SEM results showing that the APSAC morphology is heterogeneous and the FTIR results indicating that more than one type of oxygenated group takes part in binding Cr(VI).

Table 7. Non-linear isotherm parameters for Cr^{2+} adsorption onto APSAC

Isotherm model	Non-linear equation	Parameter	Result
Langmuir	$q_e = \frac{q_m b C_e}{1 + b C_e}$	q_m b R^2	0.262286408 2.436677744 0.910552
Freundlich	$q_e = k_f C_e^{1/n}$	k_f n R^2	1.069607895 0.903538479 0.916494
Sips	$q_e = \frac{q_{ms} K_s C_e^{\beta}}{1 + K_s C_e^{\beta}}$	q_{ms} K_s β R^2	0.006970026 11241417.68 3.085929447 0.984892
Redlich–Peterson	$q_e = \frac{A C_e}{1 + B C_e^{\beta}}$	A B β R^2	0.629934119 1.253338793 1.571175204 0.911054

3.9. Kinetics of adsorption and diffusion mechanism

Parameters describing the kinetics of chromium sorption by APSAC have been presented in Table 8. The pseudo first order equation provided slightly better fitting to the data compared to the pseudo second order equation ($R^2 = 0.9427$ vs $R^2 = 0.9421$). Nevertheless, this slight difference indicates that surface adsorption was one of the important steps in the chromium sorption process. Nevertheless, similarity in these two equations shows that the process could not be described in terms of either physical adsorption or chemisorption only [29,30].

Table 8. Kinetic parameters for Cr^{2+} adsorption onto APSAC

Kinetic model	Non-linear equation	Parameter	Result
Pseudo-first-order	$q_t = q_e \left(1 - e^{-K_1 t}\right)$	K_1 q_e R^2	1.46265×10^{-5} 5.148106443 0.94268
Pseudo-second-order	$\frac{dq_t}{dt} = K_2 (q_e - q_t)^2$	K_2 q_e R^2	6.54372×10^{-5} 1.07455087 0.94207
Intra-particle diffusion	$q_t = K_p \sqrt{t} + C$	K_{ip} C R^2	0.000534207 0 0.762849
Boyd	$F = 1 - \frac{6}{\pi^2} \sum_{n=1}^{\infty} \left(\frac{1}{n^2}\right) \exp(-n^2 B t)$	q_e R^2	5.1481 0.9748

The intra-particle diffusion model resulted in an R^2 value of 0.7628, which shows that pore diffusion was not entirely responsible for the rate of adsorption. The Boyd model offered the best fit ($R^2 = 0.9748$), while the graph obtained for the Boyd model in Figure 6 does not start from zero. This means that film diffusion played a major role in the adsorption of chromium ions [31]. Therefore, the process scale-up must account for mixing intensity, contact effectiveness, and adsorbent dispersion, apart from equilibrium capacity.

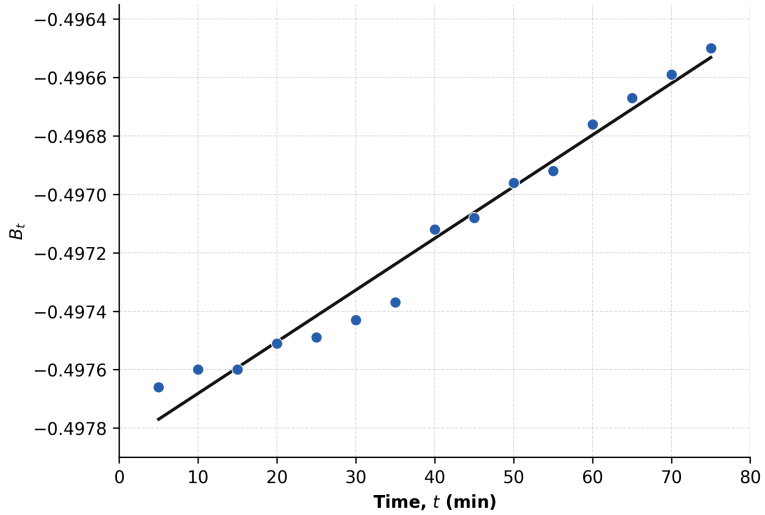

Figure 6. Boyd-model plot for Cr^{2+} adsorption onto APSAC

4. Conclusion

The current research attempted to find out whether African pear seed activated carbon could be used as an efficient adsorbent for the removal of chromium from brewery effluent. In addition, it sought to establish the factors and mechanisms behind the adsorption activity of the material. The results of this study are affirmative in answering the above-stated objective. APSAC obtained through acid assisted activation showed very low moisture content, ash content, and very high fixed carbon content, as well as a rough and porous nature and oxygen-containing functional groups on the surface for chromium binding.

The response surface method gave the information that removal efficiency and adsorption capacity had to be considered together since a high percentage of removal does not guarantee maximum adsorption capacity. The significant adsorption-capacity model ($R^2 = 0.9617$) indicated that dosage and non-linear factor effects were important for obtaining an appropriate operating range. Equilibrium study showed that the Sips isotherm model was the most representative in describing the adsorption process, which indicated the heterogeneous surface binding. Kinetic and Boyd methods revealed the surface and film diffusion mechanisms to be responsible for the chromium adsorption. The results have proved APSAC to be a potential adsorbent for chromium removal in beer wastewater and have provided a foundation for future research on its regeneration and operational performances.

Abbreviations

APSAC	African pear seed activated carbon
ANOVA	Analysis of variance
AAS	Atomic absorption spectroscopy
ASTM	American Society for Testing and Materials
CCD	Central composite design
DOE	Design of experiment
FTIR	Fourier-transform infrared spectroscopy
PFO	Pseudo-first-order
PSO	Pseudo-second-order
RSM	Response surface methodology
SEM	Scanning electron microscopy
TDS	Total dissolved solids

References

[1] Folorunsho, A. T., Abel, U. A., & Promise, E. U. (2016). A Statistical Approach to Optimization of Congo Red Dye Removal (CRDR) Via Coconut Shell Activated Carbon (CSAC). *International Journal of Computational and Theoretical Chemistry, 4*(7), 7-13.

[2] Folorunsho, A. T., Isotuk, U. R., & Job, A. I. (2026). Modelling and Optimization of the Removal of Congo-Red Dye from Waste Water Using Agricultural Waste. *Journal of Chemical, Environmental and Biological Engineering, 1*(1), 11–17.

[3] Juturu, R., Vinayagam, R., Murugesan, G., & Selvaraj, R. (2025). Enhanced adsorptive removal of chromium (VI) ions from wastewater with phosphorus-doped magnetite-carbon composite: advanced statistical physics modeling and kinetic studies. *Environment, Development and Sustainability,* 1-27.

[4] Kanu, I., & Achi, O. K. (2011). Industrial effluents and their impact on water quality of receiving rivers in Nigeria. *Journal of Applied Technology in Environmental Sanitation, 1*(1), 75-86.

[5] Godwin, O. O. (2017). Telfairia occidentalis Hook. F. Grown on Crude Oil Polluted Soil. *American Journal of Agricultural Science, 4*(4), 88-93.

[6] Saad, E. M., Abd-Elhafiz, M. F., Ahmed, E. M., & Markeb, A. A. (2024). Hexavalent chromium ion removal from wastewater using novel nanocomposite based on the impregnation of zero-valent iron nanoparticles into polyurethane foam. *Scientific Reports, 14*(1), 5387.

[7] Abel, U. A., Habor, G. R., & Oseribho, O. I. (2020). Adsorption studies of oil spill clean-up using coconut coir activated carbon (CCAC). *American Journal of Chemical Engineering, 8*(2), 36-47.

[8] Enitan, A. M., Adeyemo, J., Kumari, S., Swalaha, F. M., & Bux, F. (2015). Characterization of brewery wastewater composition. *International Journal of Environmental and Ecological Engineering, 9*(9), 1073–1076.

[9] Gupta, G., Khan, J., & Singh, N. K. (2021). Application and efficacy of low-cost adsorbents for metal removal from contaminated water: A review. *Materials Today: Proceedings, 43*, 2958-2964.

[10] Akpan, S., & Umana, S. U. (2022). Characterization of physico-chemical properties and heavy metal concentrations of surface water receiving effluent from Champion Breweries PLC in Uyo, Akwa Ibom State, Nigeria. *Global Sustainability Research, 1*, 5–13.

[11] Akinterinwa, A., & Adebayo, I. (2018). Chemical Precipitation Approach to the Removal of Heavy Metals from Wastewater for Discharge into Sanitary Sewerage. *International Journal of Chemistry, 1*, 2581–7760.

[12] Tawila, Z. M. A., Ismail, S., Amr, S. S. A., & Abou Elkhair, E. K. (2019). A novel efficient bioflocculant QZ-7 for the removal of heavy metals from industrial wastewater. *RSC Advances, 9*(48), 27825-27834.

[13] Velarde, L., Nabavi, M. S., Escalera, E., Antti, M. L., & Akhtar, F. (2023). Adsorption of heavy metals on natural zeolites: A review. *Chemosphere, 328*, 138508.

[14] Fungaro, D. A., Borrely, S. I., & Carvalho, T. E. (2013). Surfactant modified zeolite from cyclone ash as adsorbent for removal of reactive orange 16 from aqueous solution. *American Journal of Environmental Protection, 1*(1), 1-9.

[15] Ukpong, A. A., Edekhe, G. I., & Asuquo, E. O. (2024). The Adsorption Studies for the Removal of Lead (Pb2+) from Paint Industrial Wastewater using Avocado Seed Activated Carbon (ASAC). *International Journal of Research and Scientific Innovation (IJRSI), 1*(11), 414-425.

[16] Köseoğlu, E., & Akmil-Başar, C. (2015). Preparation, structural evaluation and adsorptive properties of activated carbon from agricultural waste biomass. *Advanced Powder Technology, 26*(3), 811-818.

[17] Benmahdi, F., Khettaf, S., & Kolli, M. (2024). Efficient removal of Cr (VI) from aqueous solution using activated carbon synthesized from silver berry seeds: modeling and optimization using central composite design. *Biomass Conversion and Biorefinery, 14*(5), 7087-7101.

[18] Dhahri, R., Yılmaz, M., Mechi, L., Alsukaibi, A. K. D., Alimi, F., ben Salem, R., & Moussaoui, Y. (2022). Optimization of the preparation of activated carbon from prickly pear seed cake for the removal of lead and cadmium ions from aqueous solution. *Sustainability, 14*(6), 3245.

[19] El Maguana, Y., Elhadiri, N., Bouchdoug, M., Benchanaa, M., & Jaouad, A. (2019). Activated carbon from prickly pear seed cake: optimization of preparation conditions using experimental design and its application in dye removal. *International Journal of Chemical Engineering, 2019*(1), 8621951.

[20] Abel, U. A., Ekanem, O. G., Oseribho, O. I., Isotuk, U. R., Job, A. I., & Ibanga, I. U. (2024). Enhanced Hydrophobicity and Oleophilicity of Modified Activated Carbons Derived from Agro-Wastes Biomass for the Removal of Crude Oil from Aqueous Medium. *American Journal of Chemical Engineering, 12*(4), 80-96.

[21] Saleem, M. (2024). Sustainable production of activated carbon from indigenous Acacia etbaica tree branches employing microwave induced and low temperature activation. *Heliyon, 10*(2), e24113.

[22] Bouzgarrou, S. M., Jedli, H., Hassani, R., Sabi, E., Khan, A. H., & Slimi, K. (2025). Experiments and physical Investigation on the adsorption of methylene on activated carbon. *Scientific Reports, 15*, 45075.

[23] Ibrahim, Y., Naddeo, V., Banat, F., & Hasan, S. W. (2020). Preparation of novel polyvinylidene fluoride (PVDF)-Tin (IV) oxide (SnO2) ion exchange mixed matrix membranes for the removal of heavy metals from aqueous solutions. *Separation and Purification Technology, 250*, 117250.

[24] Younas, F., Bibi, I., Afzal, M., Al-Misned, F., Niazi, N. K., Hussain, K., ... & Wang, H. (2023). Unveiling distribution, hydrogeochemical behavior and environmental risk of chromium in tannery wastewater. *Water, 15*(3), 391.

[25] Abuilaiwi, F. A. (2020). Removal of Cadmium (II), Chromium (III), and Lead (II) Heavy Metal Ions from Water by Graft Copolymerization of Acrylonitrile onto Date Palm Fiber Using H2O2/Fe++ as an Initiator. *International Journal of Polymer Science, 2020*(1), 1239267.

[26] Naushad, M., Ahamad, T., Alothman, Z. A., Shar, M. A., AlHokbany, N. S., & Alshehri, S. M. (2015). characterization and application of curcumin formaldehyde resin for the removal of Cd^{2+} from wastewater: Kinetics, isotherms and thermodynamic studies. *Journal of Industrial and Engineering Chemistry, 29*, 78–86.

[27] Foo, K. Y., & Hameed, B. H. (2010). Insights into the modeling of adsorption isotherm systems. *Chemical Engineering Journal, 156*(1), 2-10.

[28] Al-Ghouti, M. A., & Da'ana, D. A. (2020). Guidelines for the use and interpretation of adsorption isotherm models: A review. *Journal of Hazardous Materials, 393*, 122383.

[29] Zewail, T. M., & Yousef, N. S. (2015). Kinetic study of heavy metal ions removal by ion exchange in batch conical air spouted bed. *Alexandria Engineering Journal, 54*(1), 83-90.

[30] Wang, J., & Guo, X. (2020). Adsorption kinetic models: Physical meanings, applications, and solving methods. *Journal of Hazardous Materials, 390*, 122156.

[31] Bulut, Y. (2007). Removal of heavy metals from aqueous solution by sawdust adsorption. *Journal of Environmental Sciences, 19*(2), 160-166.